ON THE ONGOING MULTIPLE BLOWOUT IN NGC 604

GUILLERMO TENORIO-TAGLE

Instituto Nacional de Astrofísica, Optica y Electronica, Apartado Postal 51y216, Puebla, Puebla 72840, Mexico

CASIANA MUÑOZ-TUÑÓN

Instituto de Astrofísica de Canarias, Via Lactea, E-38200 La Laguna, Tenerife, Spain

ENRIQUE PÉREZ

Instituto de Astrofísica de Andalucía (CSIC), Apdo Correos 3004, Granada, E-18080, Spain

JESÚS MAÍZ-APELLÁNIZ

Space Telescope Science Institute, 3700 San Martin Drive, Baltimore, MD 21218, and Laboratorio de Astrofísica Espacial y Física Fundamental-INTA, Apartado Postal 50727, 28080 Madrid, Spain

AND

GUSTAVO MEDINA-TANCO

Instituto Astronômico e Geofísico, Deaprtment of Astronomy, University of São Paulo, Caixa Postal 3386, São Paulo, SP 01060-970, Brazil

ABSTRACT

Several facts regarding the structure of NGC 604 are examined here. The three main cavities produced by the mechanical energy from massive stars, which in NGC 604 are spread over a volume of 10^6 pc^3, are shown here to be undergoing blowout into the halo of M33. High-resolution long-slit spectroscopy is used to track the impact from massive stars, while *Hubble Space Telescope* archive data are used to display the asymmetry of the nebula. NGC 604 is found to be a collection of photoionized filaments and sections of shells that are in direct contact with the thermalized matter ejected by the massive stars. The multiple blowout events presently drain the energy injected by massive stars, and thus the densest photoionized gas is found almost at rest and is expected to suffer a slow evolution.

Subject headings: galaxies: ISM — H II regions — ISM: individual (NGC 604) — ISM: kinematics and dynamics

1. INTRODUCTION

Upon the formation of massive stellar clusters, the energy input from massive stars leads to a rapid structuring of the surrounding medium. This was originally thought to be due to the high pressure acquired by the constant density photoionized gas which, upon the formation of the H II region, would expand with a speed smaller than the sound speed ($c_{H\,II} \sim 10$ km s^{-1}) onto the surrounding neutral gas to acquire a radius

$$R_{H\,II}(t) = R_S[1 + 7/4(c_{H\,II}\,t/R_S)]^{4/7}$$

where R_S is the Strömgren radius (Spitzer 1968; Osterbrock 1989). Much larger speeds were envisaged in "champagne flows" as a result of the pressure gradient between the photoionized parent cloud and the photoionized intercloud medium, established suddenly as the ionization front (either D or R type) overruns the parent cloud edge (Tenorio-Tagle 1979). In this case the ionization front rushes to infinity, and strong isothermal shocks develop within the photoionized region. The shocks are driven by the ionized cloud matter that supersonically streams into the intercloud medium in an attempt to lift and equalize the pressure between the two regions. The champagne phase would then last until the pressure gradient is smoothed out, which is only accomplished once the whole ionized cloud is dispersed.

A completely new paradigm resulted from taking into consideration the mechanical energy produced by massive stars and the evolution of superbubbles. In this case three concentric distinct regions were shown to develop around the exciting source (Castor, McCray, & Weaver 1975). The central region (*a*) contains the hypersonic wind from the massive star(s). At a certain radius R_a the hypersonic wind is abruptly thermalized at a reverse shock. The speed of the wind, the high temperature [$T = 1.4 \times 10^7$ ($v_{wind}/1000$ km s^{-1})^2 K $\sim 10^6$–10^7 K], and the high pressure acquired upon thermalization allow the shocked wind to fill a large volume (region *b*) while driving a strong shock into the surrounding gas. The latter shock then sweeps and accelerates the surrounding interstellar medium (ISM) into a dense expanding shell (region *c*) that grows as a function of time (Castor et al. 1975; Weaver et al. 1977):

$$R_s(t) = 0.76(\dot{E}/\rho)^{1/5}t^{3/5} ,$$

where $\dot{E}$ is the mechanical energy input rate and ρ is the mass density of the background medium. Castor et al. (1975) also showed that, given the number of recombinations within the expanding shell and its rapid growth, the ionization front became trapped within the shell early in the evolution of the system. This was shown to happen despite the fact that most of the volume is filled with the hot thermalized wind, which is a transparent medium to the ionizing photon flux because of its high temperature. Consequently, the H II region gas in this model was shown to be rapidly confined to a narrow, two-dimensional structure within the expanding shell.

Other models that account only for the mechanical energy deposited by OB associations and starbursts (Tenorio-Tagle & Bodenheimer 1988) have clearly shown how the shells of swept-up matter can easily be disrupted upon crossing a large density gradient. This phenomenon, commonly referred to as blowout, occurs as a shell suffers a sudden acceleration, which drives it Rayleigh-Taylor unstable and causes its rapid fragmentation. The event then leads to the venting of the hot superbubble interior onto the low-density gas where a new shell of halo swept-up matter will develop. More recent studies have also shown that the

blowout also leads to the escape of the UV photons, which otherwise would be trapped within the decelerating shell. The escape of ionizing radiation has been shown to lead to the development of an extended, low-surface brightness conical H II region ahead of the superbubble-leading shock (Tenorio-Tagle et al. 1999).

Here we focus our attention on the nearest northern hemisphere giant H II region NGC 604. The giant nebula is the largest in the neighboring spiral galaxy M33 (at a distance of 840 kpc; Freedman, Wilson, & Madore 1991) and is located in one of the spiral arms, 2.4 kpc from the galaxy center. Looking at NGC 604 it is quite evident that it is not a spherical nebula. It presents a large number of shells, filaments, or arches of a wide variety of lengths and intensities. Its general appearance is, however, very similar to other giant H II regions, in particular to the 30 Doradus Nebula. The large number of shells and networks of shells in 30 Doradus have been identified spectroscopically by Chu & Kennicutt (1994). Such a structure, i.e., expanding shells within shells, implies a very inhomogeneous, rapidly structured or prestructured parent cloud density distribution. An endless number of tunnels or cavities, across which the thermalized winds from the massive stars could freely flow causing their expansion and further growth, allows for the appearance of a network of nested shells in projection. In such a case, the thermalized ejecta and the hot coronal gas would be in direct contact with the H II region gas, and the latter would be confined to the narrow, denser walls of the network of tunnels or to the sections of the expanding shells, thus presenting a three-dimensional superposition of multiple two-dimensional structures.

Here we analyze the ionization structure and the velocity field of NGC 604 with the aim of unveiling its true morphology and the possible evolution of the nebula. In § 2 we analyze the two data sets used in this work, and in § 3 we present a discussion of the results and our conclusions.

2. ANALYSIS AND RESULTS

2.1. *Hubble Space Telescope Imaging*

We have retrieved from the *HST* archives the narrow-band images in the emission-line filters of Hα (F656N), [O III] λ5007 (F502N), and [S II] λ6717 + 6731 (F673N). Each final image is the combination of two 1100 s exposures using the STSDAS tasks CRREJ and WCOMBINE. Figure 1 shows the image ratios corresponding to [O III]/Hα and [S II]/Hα.

A cursory look at these two image ratios shows that, as expected, they trace distinctly different regions of the nebula. The [S II]/Hα ratio traces the low-excitation regions and is not affected by extinction. The [O III]/Hα ratio traces the high-excitation regions, but it can be affected by extinction, so that a high value always indicates high excitation, but a low value can be a combination of both low excitation and/or high extinction. This technique of using narrowband emission-line imaging ratios has been used successfully in the literature to study the ionization structure and the radiation field in different types of photoionized sources, such as Seyfert and starburst galaxies, where ionization cones and other collimated structures have thus been uncovered (Tadhunter & Tsvetanov 1989; Pérez et al. 1989).

The high-excitation O^{++} region is maintained by radiation with at least 35 eV, while the low-excitation S^+ zone requires only photons more energetic than 10 eV. Thus in an idealized constant density H II region with a source of UV photons arising from the center of the nebula the S^+ zone should be concentric and surrounding the O^{++} zone. This is clearly not the case in NGC 604 (see Fig. 1). Instead, although the high-excitation region is largely confined by the outer low-excitation region, there exists a large, almost straight dividing line that spans across ~200 pc (50″), almost through the center of the nebula (offset by some 10″), and runs from the extreme northern to the southern edge. The sharp boundary between the two emitting volumes (hereafter referred to as the "ridge") has no explanation within the standard case. Note, however, that (unlike R136 in 30 Doradus) the ionizing cluster in NGC 604 is not centrally concentrated, but rather the 186 massive O stars visible in the *HST* images are here distributed over a projected area of about 10,000 pc² (Hunter et al. 1996; Terlevich et al. 1996; see Fig. 2 in González-Delgado & Pérez 2000). Furthermore, from a recent radio continuum and Hα study, Churchwell & Goss (1999) conclude that the main emission centers (their knots A–F) are also photoionized from the inside by heavily obscured massive stars, and an average of five or more O stars are required to produce the ionization of each of the condensations. These come to enhance the number of massive O stars to more than 220 scattered over the projected central 10,000 pc² area. Also from this work an extinction map was obtained with values ranging from 0.3 to 0.5 mag, thus implying that we see most of the nebula without obscuration (see also Díaz et al. 1987). Another recent analysis (Maíz-Apellániz, Pérez, & Mas-Hesse 2000, in preparation) finds a discrepancy between the extinction measured from the Balmer decrement and the one found by Churchwell & Goss (1999), suggesting that a large fraction of the obscuring dust is mixed with or located close to the gas. This, together with the CO detection (Viallefond & Goss 1986), implies that a molecular cloud exists behind the photoionized nebula NGC 604.

The length of the ridge between the two different excitation regions demands the existence of a sharp discontinuity across which distinct physical conditions operate and which is most likely caused by the existence of a molecular wall (Wilson & Scoville 1992; Maíz-Apellániz et al. 2000, in preparation). The ridge, seen in deep Hα images, seems to result from the chance alignment of the three main shells, or superbubbles, whose sharp and elongated edges coincide to give the appearance of a long ridge (see Figs. 1 and 2).

Further information regarding the structure of the region can be derived from the kinematics of the ionized gas. In what follows we analyze spectra taken with the William Herschel Telescope (4.2 m) at the Observatorio del Roque de los Muchachos using the double-arm ISIS spectrograph.

2.2. *The Peak Intensity Features*

A 1″ wide slit was placed east-west at 10 different locations that were stepped by 2″ or 3″ across the nebula (the step between slit positions 6 and 7 is 2″). The sampling along the spectral and spatial direction in the slit is 0.37 Å pixel^{-1} and 0.″33 pixel^{-1}, respectively. The precise location of the slits is shown in Figure 2, and a detailed description of the observational setup and data reduction can be found in Mas-Hesse et al. (1994), Maíz-Apellániz (1999), and Maíz-Apellániz et al. (1999). Figures 3a–3j display the measured velocity and flux of the Hα emission line along each of the slits that cross the nebula. The measurements have been made by fitting a single Gaussian component to the
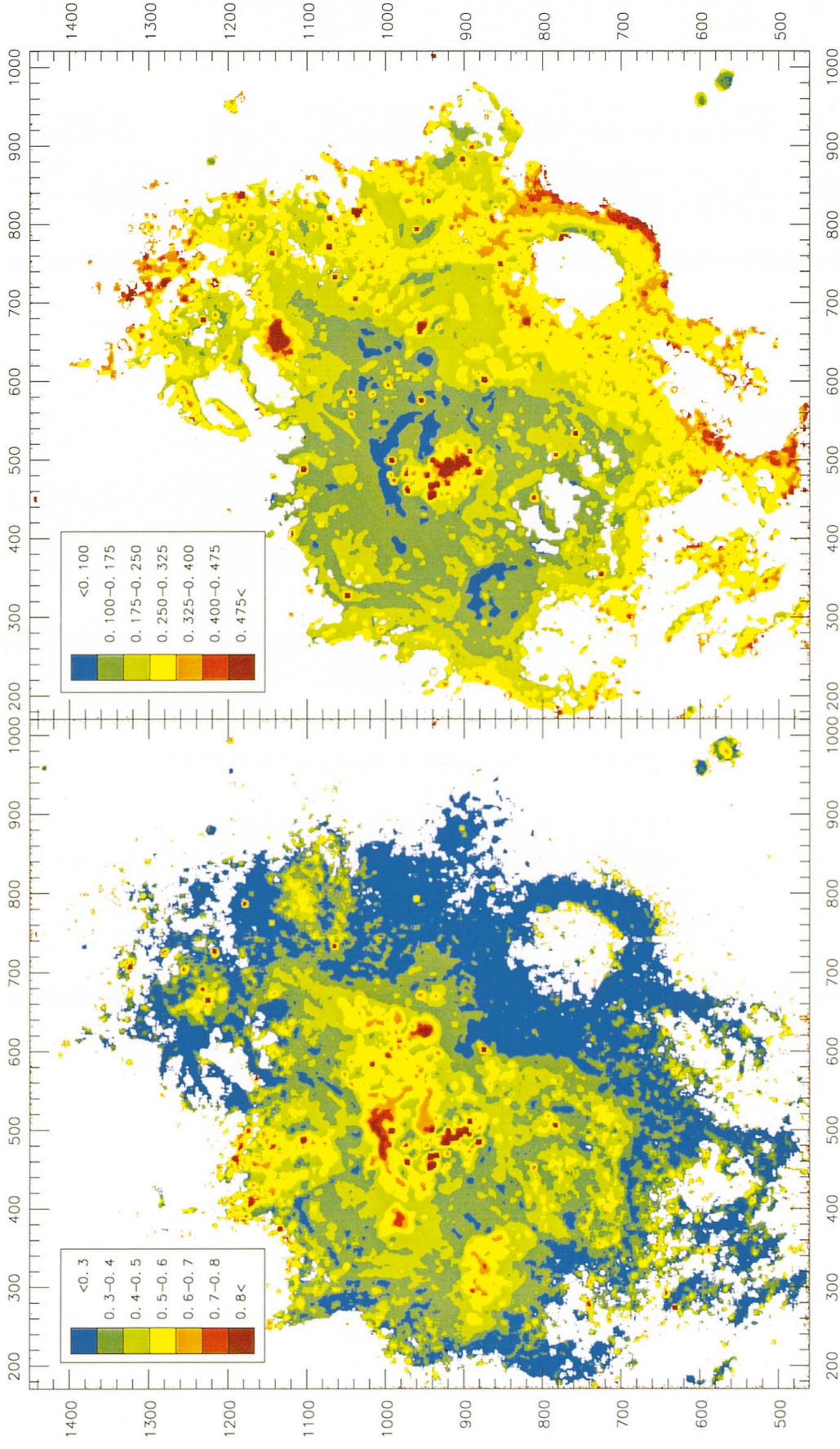
FIG. 1.—[O III]/Hα (*left*) and [S II]/Hα (*right*) excitation maps derived from the *HST* WFPC2 images of NGC 604. The scale used for each of the ratios is indicated in the legend. Note that for [O III]/Hα, high values correspond to high excitation, while for [S II]/Hα, high values correspond to low excitation. The axes are labeled in WF pixels, with 1 pixel ≈ 0″.1. North points toward the lower left corner, forming an angle of 27°.72 with the vertical.
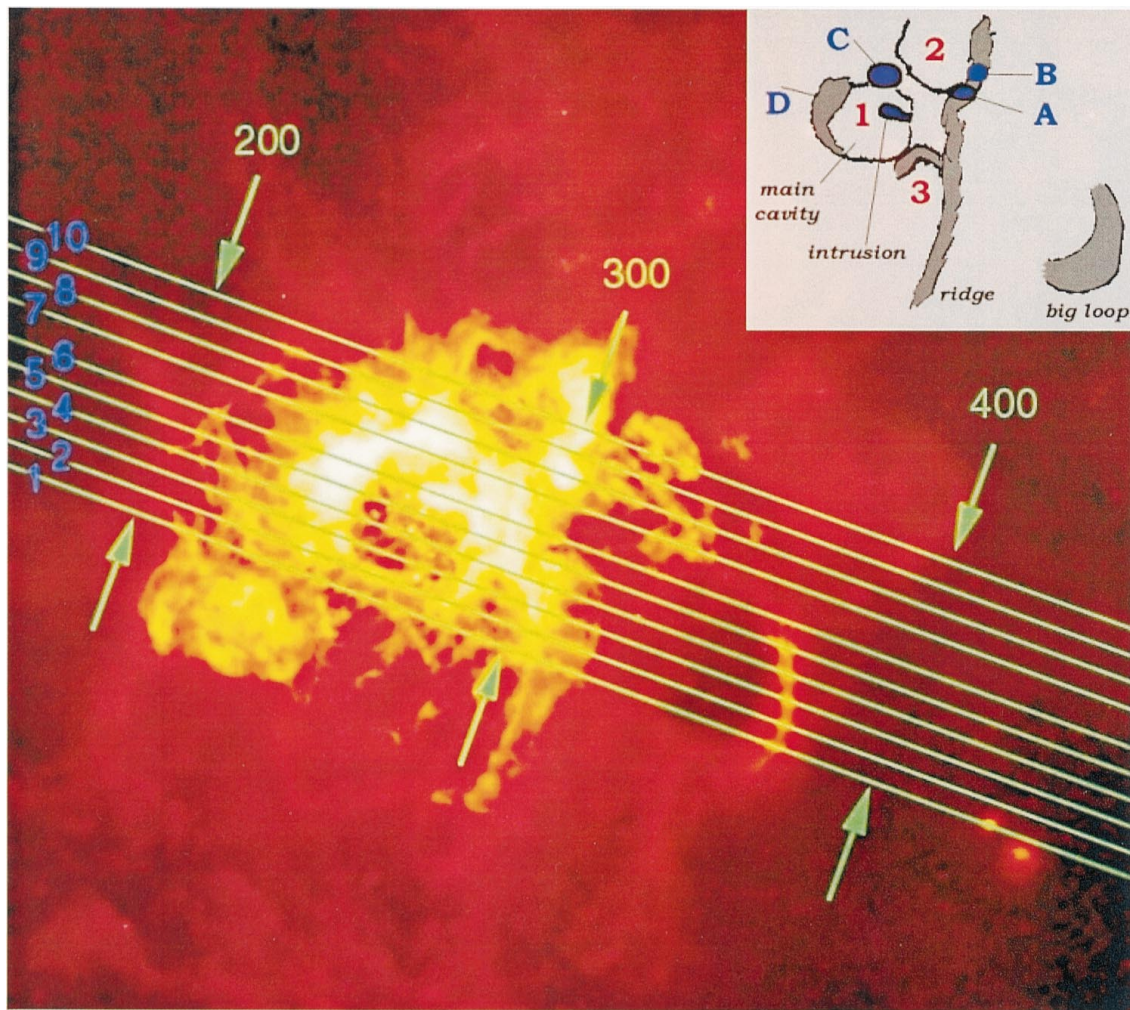
Fig. 2.—NGC 604 *HST* Hα image with overlaid slit locations. The inset sketches the main features discussed in the text.

observed Hα emission line except where a good fit to the line required two or sometimes three components. The velocity field (km s^{-1}) is derived from the center of the Gaussian fits, referred to as the Hα rest wavelength ($\lambda_0 =$ 6562.58 Å). The line intensity scale (in arbitrary units) gives an indication of the density, or the column density, at the observed locations. The median velocity is 256 ± 9 km s^{-1}.

The long ridge that divides the east and west sides of the nebula is evident in all of the slits. The feature presents a maximum intensity at pixel ~ 300 on all slits. The central velocity at such local maxima is very uniform with values of -250 to -260 km s^{-1} across the 10 slits. These are very similar to the local galaxy reference frame velocity. The sharp ridge across the nebula is most probably a high-density wall with a very steep drop in intensity toward the east, which is noticeable on all slits. Much further away (around location 370) one finds the Big Loop. This is easily identified in Figure 2 across slits 1–5 (*see inset sketch*).

Further out on slit 1, at positions 430 and 445, the two small local maxima correspond to two small H II regions (Fig. 2), and both also present a velocity of -260 km s^{-1}. The two pointlike H II regions have been used as a reference for the positioning of the slits.

Churchwell & Goss (1999) have identified six radio continuum maxima and labelled them as A–F. In what follows we shall keep their nomenclature (see Fig. 2). The brightest

zones of the nebula are crossed by slits 6–10. The sharpest peak is knot A, which is easily found on slit 8 at pixel 300. Its spatial extent, measured as the apparent width at half-intensity, is about 5 pixels, or 1".8, equivalent to 7.9 pc if one assumes a distance scale of 4.1 pc arcsec^{-1}. Knots A and B (on slits 8, 9, and 10) lie on top of a high-density wall, and, in fact, between them form the most evident southern part of the long ridge.

The other main emitting knots are also clear in our spectra. Knot D is very elongated and most evident on slits 4–7. It is brighter on slit 6 (with 10^4 counts at position 245) and of comparable brightness on slit 7 (9000 counts at 250). The intensity of this features slowly fades through slits 5 (5500 counts at 245), 4 (3200 counts at 240), 3 (2300 counts at 245), and 2 (1700 counts at 240), and it is absent on slit 1. A deep inspection of the image shows, in fact, that the feature ends up running almost parallel to slit 2 (from position 250 to 280). Therefore, although along the slit direction knot D is relatively narrow (~ 15 pixels wide at half-intensity on slit 7) it extends continuously from the northwest northward and then to the east following a concave curvature. The emission increases once again as one moves toward the south across slits 3–7 (positions 280–290). Toward the south the feature acquires large intensity values, similar to those found along the extension of knot D toward the north. If one follows this roundish shape moving
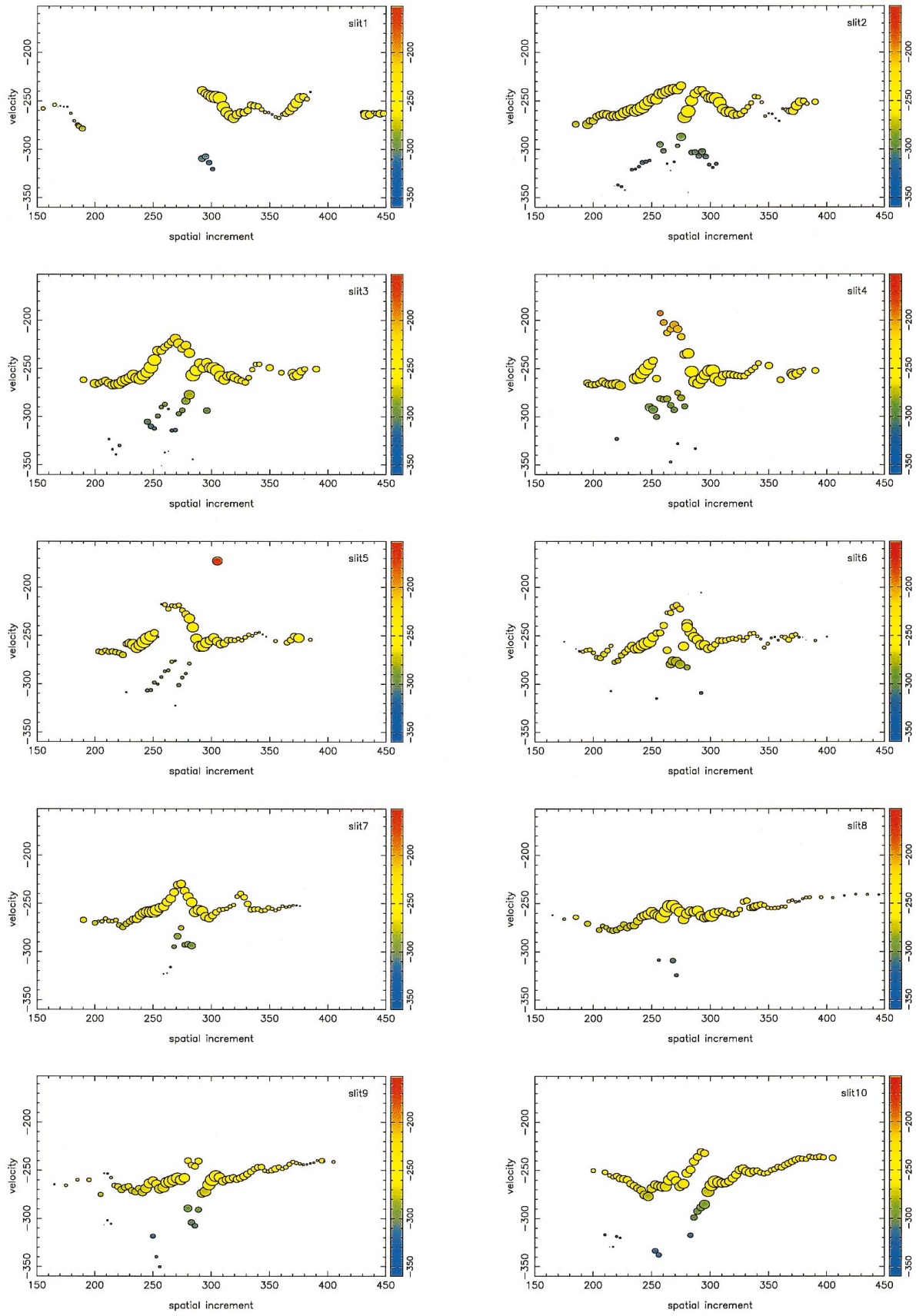
FIG. 3.—Hα velocity along the 10 slit positions across the nebula. The size of the symbol is proportional to the log of the Hα flux within that slit position. The vertical scale is in units of km s^{-1}, and the horizontal scale is in long-slit pixels (1 pixel ≈ 1.3 pc).

onto slit 8, one finds the next maximum in intensity (knot C). In our spectra this splits into two distinct knots, each of them with typical sizes of 10 pixels ($\sim 3\farcs 7$ width at half-intensity) equivalent to 15.2 pc.

With the exception of knots A and B the intensity maxima described above clearly define a central zone with a much lower Hα intensity. There the flux measured in between maxima reaches the lowest possible values (as on slits 4 and 5). There seems to be an empty hole, the boundary of which is well delineated by some of the main emitting knots and by the slightly curved central section of the ridge on the east side. We have then identified an elliptically shaped cavity with a diameter of ~ 40 pixels (~ 15 arcsec $\times$ 11.25 arcsec or 61.5 pc $\times$ 46.2 pc).

Within the central hole we identify a small but extended zone (the "intrusion"), which extends (east-west) from pixel 300 to 265 along slit 6, i.e., some 15 pixels (22.75 pc) while reaching a maximum flux of 2500 units.

2.3. The Velocity Field

The two reference H II regions (at pixels 435 and 445 on slit 1), both ends of every slit, and all of the obvious intensity maxima traversed by the slits (with the exception of the intrusion in the main cavity) show the same velocity, -255 ± 10 km s^{-1}. This value has then been taken as the galaxy reference frame.

The velocity curves also display a different trend between the [S II] and the [O III] dominated regions. There is no zone within the east side of the [S II] region that shows line splitting. All slit positions within this [S II] dominated region, regardless of the Hα intensity, are well fitted with a single-Gaussian fit, with peak velocities of about -260 to -280 km s^{-1}, all within 10 km s^{-1} from the rest-frame velocity of M33.

One can therefore conclude that there are no signs that this region is affected by the mechanical energy from the massive stars. In fact, the [S II] zone presents evidence of a slow radial expansion with respect to the M33 reference frame velocity. Note also that not even the largest loop of NGC 604, apparent at all wavelengths at the outer edge of the nebula (at the extreme northeast edge, across slits 1–6), presents any sign of line splitting, and thus we regard it as an old structure at the edge of a molecular cloud. The exact opposite is true within the [O III] dominated zone. There the velocity field, through large line splitting, evidences the mechanical power from massive stars capable of displacing the ISM as it generates giant cavities.

Apart from the obvious main cavity there are also several smaller, less obvious holes, the borders of which are also traced in the *HST* Hα image. The largest ones (cavities 2 and 3; see Fig. 2) are to the south and north, immediately adjacent to the rim of the central hole, and are bound on their eastern side by the ridge. The two of them fade away in opposite directions; cavity 2 appears open and fainter toward the south (see slits 8–10 at pixels 260–300), while cavity 3 appears open and fainter toward the north (see slits 1–3 at pixels 280–300). Other even smaller and fainter features are even less apparent, and it is difficult to describe them with the same accuracy.

Line splitting has been detected in all three cavities. The largest expansions inferred from the spectroscopic data are ~ 100 km s^{-1} with respect to the galaxy rest frame. In the regions of line splitting the two line components are displaced from the galaxy rest frame velocity. In all cases the redshifted component acquires a maximum value of ~ -240 km s^{-1}. The redshifted component is also the one that invariably presents the largest intensity, with the exception of those arising from the intrusion feature in the main cavity. On the other hand, the blueshifted components reach values of -370 km s^{-1}, implying expansion speeds of up to 100 km s^{-1} with respect to the galaxy rest frame. In all cases the blueshifted components also present a low-intensity flux that is always below 100 counts (see Fig. 3) except in the intrusion feature seen in the projection within the main cavity. The intrusion thus appears as a dense feature (with an intensity of ~ 2000 counts at pixel 270 on slit 6) that is blueshifted some 20 km s^{-1} with respect to the galaxy rest frame velocity. At the same position the red-shifted counterpart reaches speeds of ~ -220 km s^{-1}, very similar to those detected at the same pixel location on the neighboring slits 5 and 7. There are also some regions, very few, that display more than two components. These are all found within the main cavity. A precise modeling of these is difficult to do, particularly when the measured parameters are affected by large uncertainties. All one can assure is that more than two Gaussian components are required to reproduce the emission line profile. We must certainly be intercepting remnant shells or low-intensity filaments along the line of sight, stressing the idea of depth or of a three-dimensional structure of the nebula.

Note, however, that the velocity centroids of the split lines do not conform in any of the studied cases to complete velocity ellipsoids, as would be expected from an ionized shell expanding into a uniform density medium [i.e., as one approaches the borders of the expanding structure, an ellipsoid that shows a maximum speed of approach and recession when looking across the center of the cavities while steadily merging with the galaxy rest-frame velocity (see, e.g., Maíz-Apellániz et al. 1999)]. The data instead show distinctly open structures. Line splitting is clearly found even when looking over some of the borders, or the rims, of the most obvious cavities (see slits 2 and 3).

Figure 4 maps the velocity centroids of the two main line-splitting components across the north-south direction and through the centers of cavities 1, 2, and 3. Figure 4*a* shows the range of velocities detected at pixel 270. Figures 4*b* and 4*c* show the trend of the blueshifted and the red-shifted components in cavities 2 (pixel 285) and 3 (pixel 290), respectively. In the three cases the velocity ellipsoids that are expected from shelllike structures expanding onto the parent cloud are not recovered. The line splitting shown in all of them leads to widely separated velocity features with a Δv in the range of 60–70 km s^{-1}. Following the slits across the cavities, i.e., along the east-west direction (see Fig. 3), one can see that the line splitting is confined by the borders of the cavities. Although slit 2 at position $\sim$ pixel 280 presents evidence of a large line splitting right at the high-intensity border between cavities 1 and 3. This fact indicates that the blueshifted outflows from these cavities have already managed to surpass the dimensions of the cavities that originally confined them. The trend detected in the three main cavities of NGC 604 thus resembles the trace left by the cones that channel superwinds out of starburst galaxies, as in NGC 253 and M82 (see Heckman, Armus, & Miley 1990). NGC 604, being a much smaller and weaker source, represents a small-scale version of a superwind event. However, it is a clear example of the venting of the hot superbubble content into the halo of M33 as well as of
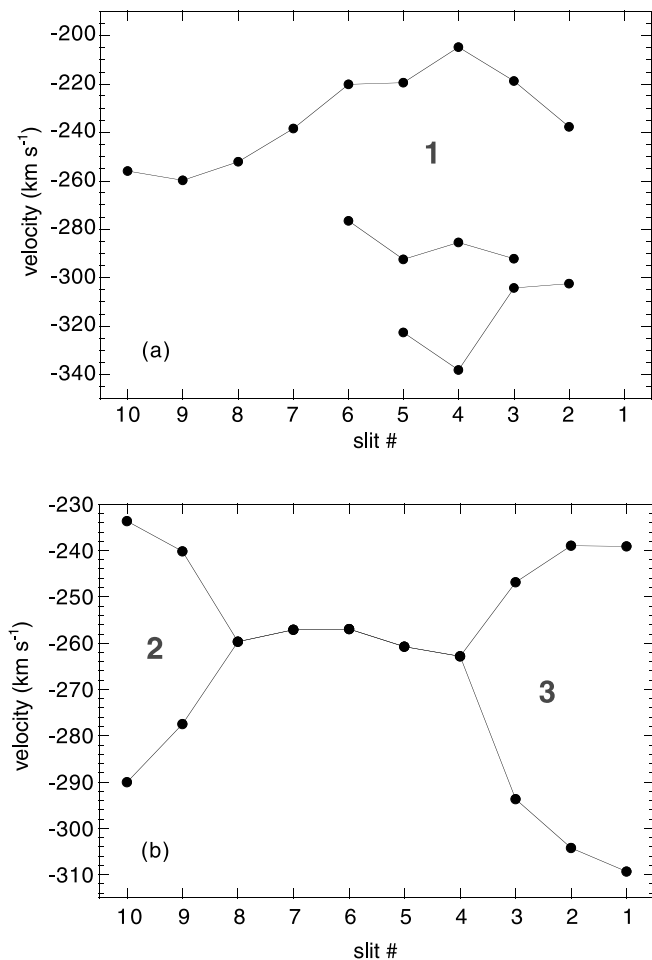
FIG. 4.—The ongoing blowout. Kinematic signatures of the three main disrupted cavities discussed in the text.

the streaming or leakage of UV radiation into the halo of M33.

Positions with line splitting associated with cavities 2 and 3 are also found at locations far from the main extended region of star formation. The line splitting at these positions appears to coincide with radial gaseous filamentary regions at the edge of the emitting zone. The structures thus resemble the tracing of conical outlets through which the hot gas, which otherwise could power the expansion of bubble-like structures, freely expands away from NGC 604, most probably into the low-density halo of M33.

The low-intensity fast blueshifted expanding components, which are much faster than those detected in the redshifted counterparts, are typical of the splitted lines. Also note that the blueshifted components present in all cases, except in the intrusion, a much lower intensity, indicative of a recent sudden burst into a lower density medium. Both of these arguments together with the fact that the blueshifted velocity component is also seen on top of the projected boundaries of the cavities (as in slits 2 and 3) support the evidence of an ongoing blowout. In this scenario the intrusion feature corresponds to the densest remaining part of a shell that has undergone blowout in our general direction. It also seems relevant to point at the elongated rim of cavity 3 that may have developed during blowout and that spans across to form the northern half length of the long ridge.

3. DISCUSSION AND CONCLUSIONS

Defining the way they evolve is central to the study of H II regions, and for this an accurate description of their morphology must be confronted with theoretical models. NGC 604 is excited by a widely spread cluster of some 200 massive stars, and these have produced two different nonconcentric excitation zones, which are also distinctly different from a kinematical point of view. Our kinematical data also provide strong evidence of an ongoing multiple blowout of the photoionized nebula into the halo of M33.

The [O III] dominated section of NGC 604 presents a corrugated multiple shell appearance, presently bursting along several directions. This is most evident across bubbles 1, 2, and 3 and along the filamentary channels detected at large radii, both along the northern and southern edges of the nebula. Note that bubbles 2 and 3 spread out far from the extended cluster of massive stars. Furthermore, in all these cases line splitting consistently shows that the densest (high-intensity) gas is only slightly redshifted with respect to the galaxy reference frame, and thus it is expected to evolve very slowly during the lifetime of the exciting stars. On the other hand, the low intensity blueshifted counterpart is clearly affected by a rapid evolution, as expected from the surface of superbubbles bursting toward us at high speeds into the halo of M33.

The eastern [S II] section of NGC 604 presents a completely different structure that seems kinematically unaffected by the winds and supernovae from the extended exciting cluster. This conclusion arises from the absence of line splitting and the lack of bubble-like structures. In fact, the [S II] region gives the impression of a large photoionized section of the surface of an extended cloud that is expanding away from us with a velocity smaller than 10 km s^{-1}.

Many models have been used to explain diffuse ionized nebulae (see § 1). However, to account for the observed facts above a particular scenario is required. This involves a pillar morphology of the parent molecular cloud where massive star formation must have been triggered at one end and deep along its surface, perhaps by a major disturbance such as the M33 spiral density wave. The star formation event covers in projection an area of some 10,500 pc^2 and probably must occupy a volume of $\sim 10^6$ pc^3. We envisage star formation as having occurred in many places deep enough inside the cloud and closely spaced together enough to allow the mechanical energy from massive stars to build up a network of twisted tunnels filled with the thermalized ejecta in a similar manner to that envisaged by Cox & Smith (1974) for OB associations in the galaxy. The tunnels will then traverse the tip of the giant molecular cloud and become broader, particularly in the outward direction (i.e., away from the symmetry axis or densest part of the cloud, in the places where more energy is deposited per unit time) or where the local surrounding cloud density is the lowest. In some of these places the energy from the "supertunnels" will even burst out of the cloud, releasing the hot coronal gas into the low density surrounding medium. Looking at the cloud along its symmetry axis, the enhanced diameter sections of the cylindrical tunnels would appear like the borders, or rims, of individual "shells," and the collection of protuberances along the surface of a tunnel could cause the appearance of networks of nested shells.

NGC 604 has three large cavities evident in the *HST* Hα

image. The rims of these form the broad borders of cavity 1 and of the neighboring more distorted bubbles 2 and 3. The alignment of the three borders jointly compose the dense ridge that separates the high-excitation regions from the low-excitation regions of the nebula. Note that the end of cavity 3 is the most distorted of them all and extends for some distance away from the center of star formation. The walls of the three cavities must extend deep into the cloud in order to inhibit an important leakage of hard UV radiation into the [S II] main emission section of the nebula in this way.

From the kinematic data, we know that the three main bubble structures have burst into the halo of M33, as evidenced by the line splitting across their projected cross section. This confirms the detection of the main bubbles through a completely different observational approach using Fabry-Perot data (see Muñoz-Tuñón et al. 1996). The cavities, or tunnels, also may have burst in other directions, leading to the giant faint loop structures and filamentary structures seen at large projected distances from the star forming zone. These regions, being far from the collection of exciting stars, thus present a low-ionization parameter and are most evident in [S II]/Hα.

Clearly, a detailed model of NGC 604 should strongly depart from the idealized one-dimensional spherical symmetry while allowing photoionization and the stellar wind energy input to work jointly on the shaping of the parent cloud. The above thus implies the following:

1. In NGC 604 the formation of massive stars has taken place within a large volume ($\sim 10^6$ pc^3), and the mechanical energy from these has rapidly structured the parent cloud into a collection of interconnected bubbles and tunnels filled with the thermalized matter ejected in winds and eventually supernova explosions.

2. Consequently, the H II region is not filled with photoionized gas, and thus it cannot possibly expand as was originally thought H II regions would do (see § 1). The matter surrounding massive stars has rapidly been confined to the borders or walls of the multiple bubbles and tunnels, and there exposure to the UV radiation causes the multiple shell or filamentary appearance characteristic of giant H II regions.

3. The hot coronal gas that initially drives the expansion of the network of bubbles and tunnels moves rapidly across the organized network to remain in direct contact and thus at the same pressure as the high excitation photoionized section of the nebula.

4. The evidence of blowout into the halo of M33 also implies that the expansion velocity of the tunnels and shells should rapidly plummet as the driving energy escapes into the halo of the galaxy. In this case the general structure is expected to suffer little change during the remaining lifetime of the exciting stars.

5. Blowout should allow the hot coronal medium to engulf the whole cloud and to establish a new pressure balance along the extended cloud surface.

6. Far away photoionized sections of the cloud would inevitably suffer their disruption through champagne flows, although details of such flows once the cloud surface is also permeated by the hot coronal medium remain to be worked out.

7. As a consequence of the blowout an important and increasingly larger amount of UV photons escape the nebula. This should largely contribute to the ionization of the extended halo of M33.

REFERENCES

Castor, J., McCray, R., & Weaver, R. 1975, ApJ, 200, L107
Chu, Y.-H., & Kennicutt, R. C., Jr. 1994, ApJ, 425, 720
Churchwell, E., & Goss, W. M. 1999, ApJ, 514, 188
Cox, D. P., & Smith, B. W. 1974, ApJ, 189, L105
Díaz, Á. I., Terlevich, E., Pagel, B. E. J., Vílchez, J. M., & Edmunds, M. G. 1987, MNRAS, 226, 19
Freedman, W. L., Wilson, C. D., & Madore, B. F. 1991, ApJ, 372, 455
González-Delgado, R. M., & Pérez, E. 2000, MNRAS, submitted
Heckman, T. M., Armus, L., & Miley, G. K. 1990, ApJS, 74, 833
Hunter, D. A., Baum, W. A., O'Neil, E. J., Jr., & Lynds, R. 1996, ApJ, 456, 174
Maíz-Apellániz, J. 1999, Ph. D. thesis, Univ. Complutense, Madrid
Maíz-Apellániz, J., Muñoz-Tuñón, C., Tenorio-Tagle, G., & Mas-Hesse, M. 1999, A&A, 343, 64
Mas-Hesse, M., Muñoz-Tuñón, C., Vílchez, J. M., Castañeda, H. O., & Carter, D. 1994, in Violent Star Formation: From 30 Doradus to QSOs, ed. C. U. P. G. Tenorio-Tagle (Cambridge: Cambridge Univ.), 125
Muñoz-Tuñón, C., Tenorio-Tagle, G., Castañeda, H. O., & Terlevich, R. 1996, AJ, 112, 1636

Osterbrock, D. E. 1989, Astrophysics of Gaseous Nebulae and Active Galactic Nuclei (Mill Valley: University Science Books)
Pérez, E., González-Delgado, R. M., Tadhunter, C. N., & Tsvetanov, Z. 1989, MNRAS, 241, 31P
Spitzer, L. 1968, Diffuse Matter in Space (New York: Wiley)
Tadhunter, C. N., & Tsvetanov, Z. 1989, Nature, 341, 422
Tenorio-Tagle, G. 1979, A&A, 71, 59
Tenorio-Tagle, G., & Bodenheimer, P. 1988, ARA&A, 26, 145
Tenorio-Tagle, G., Silich, S., Kunth, D., Terlevich, E., & Terlevich, R. 1999, MNRAS, 309, 332
Terlevich, E., Díaz, Á. I., Terlevich, R. J., González-Delgado, R. M., Pérez, E., & García Vargas, M. L. 1996, MNRAS, 279, 1219
Viallefond, F., & Goss, W. M. 1986, A&A, 154, 357
Weaver, R., McCray, R., Castor, J., Shapiro, P., & Moore, R. 1977, ApJ, 218, 377
Wilson, C. D., & Scoville, N. 1992, ApJ, 385, 512